Published in final edited form as:
Opt Express. 2007 December 10; 15(25): 16413–16423.

Subcellular-resolution molecular imaging within living tissue by fiber microendoscopy

Timothy J. Muldoon[1], **Mark C. Pierce**[1], **Dawn L. Nida**[1], **Michelle D. Williams**[2], **Ann Gillenwater**[3], and **Rebecca Richards-Kortum**[1,*]

[1]Dept. of Bioengineering, Rice University, 6100 Main Street, Houston TX 77005

[2]Dept. of Pathology, University of Texas M.D. Anderson Cancer Center, 1100 Holcombe Boulevard, Houston TX 77030

[3]Dept. of Head & Neck Surgery, University of Texas M.D. Anderson Cancer Center, 1100 Holcombe Boulevard, Houston TX 77030

Abstract

Conventional histopathology involves sampling, sectioning and staining of tissue specimens prior to microscopic evaluation, and provides diagnostic information at a single location and point in time. *In vivo* microscopy and molecular-targeted optical labeling are two rapidly developing fields, which together have the potential to provide anatomical and functional indications of disease by staining and imaging tissue *in situ*. To address the need for high-resolution imaging instrumentation, we have developed a compact, robust, and inexpensive fiber-optic microendoscopy system based around wide-field LED illumination, a flexible 1 mm diameter fiber-optic bundle, and a color CCD camera. We demonstrate the sub-cellular resolution imaging capabilities of the system through a series of experiments, beginning with simultaneous imaging of three different cancer cell lines in culture, each targeted with a distinct fluorescent label. We used the narrow diameter probe to access subcutaneous tumors in an *in vivo* murine model, allowing direct comparison of microendoscopy images with macroscopic images and histopathology. A surgically resected tissue specimen from the human oral cavity was imaged across the clinical margin, demonstrating qualitative and quantitative distinction between normal and cancerous tissue based on sub-cellular image features. Finally, the fiber-optic microendoscope was used on topically-stained normal human oral mucosa *in vivo*, resolving epithelial cell nuclei and membranes in real-time fluorescence images. Our results demonstrate that this imaging system can potentially complement conventional diagnostic techniques, and support efforts to translate emerging molecular-diagnostic and therapeutic agents into clinical use.

1. Introduction

In many clinical situations, visualization of cellular morphology and architecture is mandatory, requiring an excisional biopsy or fine needle aspiration to obtain tissue or cells for histopathology. Such procedures are invasive, sometimes dangerous, expensive, and the results are not immediately available. This clinical need has motivated the development of techniques for imaging tissue *in situ* with cellular resolution, aimed at complementing the pathologist's expertise though biopsy guidance and monitoring of disease progression and treatment. By analogy with chemical staining in histopathology, contrast between tissue components can be obtained *in situ* through topical or intravenous delivery of fluorescent

*Corresponding author rkortum@rice.edu.

agents. While non-specific dyes have been widely used to generate optical signals for *in vivo* imaging, an expanding array of targeted fluorescent probes are emerging that can provide indicators of disease at the cellular and molecular levels [1-4]. This ability to detect and monitor the presence and activity of disease biomarkers is expected to have considerable impact in fundamental biomedical research, and ultimately on the clinical management and care of patients [5,6]. As research in the molecular imaging field proceeds through studies in cell culture, animal models, and pre-clinical trials, robust, versatile, high-resolution optical imaging instrumentation is essential at each stage, and ultimately to accompany molecular imaging into the clinical setting.

Flexible, narrow-diameter optical fibers are well-suited for performing microscopic imaging at sites within the human body [7], and several researchers initially demonstrated the feasibility of using a length of single-mode fiber as a conduit through which confocal microscopy could be performed [8-10]. Such configurations using only a single optical fiber require a means of scanning the emerging optical beam across the specimen in order to build up an image, which to-date, still represents the overall limiting factor in system miniaturization. Scanning mechanisms based on miniature mirrors [11-13], piezoelectric actuators [14], spectral encoding [15] and electromagnetic vibration [16] have all been demonstrated, with the latter technique used to construct a scan head integrated into a standard 1.2 cm diameter clinical endoscope, providing access to hollow internal cavities including the gastrointestinal tract and colon [17-18].

A related approach that eliminates the requirement for a scanning mechanism at the distal (sample) end of a fiber, involves the use of a coherent fiber bundle, comprising thousands of individual optical fibers within a single element of sub-millimeter diameter [19,20]. The use of a coherent bundle enables the scanning mechanism to be located outside the body at the proximal end of the fiber, with the scan pattern faithfully reproduced at the distal end due to the ordered arrangement of individual fibers. The fiber bundle approach has been used for both reflectance [20,21] and fluorescence [19,22-24] confocal imaging, in both two-dimensional point scanning and one-dimensional line scanning variations [25,26]. The primary drawback of the fiber bundle approach is the appearance of the bundle structure superimposed on each image, although this artifact can be reduced by image processing methods [23,27].

In this article, we present a high-resolution fiber-optic fluorescence imaging system for visualizing sub-cellular detail in living tissue. Based on wide-field imaging through a coherent fiber bundle, all scanning requirements are eliminated, and through the use of LED illumination and CCD imaging, we have developed an inexpensive system that is both simple to implement and robust in use. We demonstrate the capabilities of the system through a series of experimental studies in biological systems, leading to *in vivo* human imaging. First, we performed multiplexed imaging of a cell-culture model containing three cancer cell lines, discriminating between cell type based on the different fluorescent markers targeted to each. We then imaged a murine tumor model *in vivo*, allowing comparison with features evident in standard macroscopic imaging and histopathology sections. Next, a surgically-resected cancerous human tissue specimen was imaged, enabling real-time visualization and quantification of cellular features across the margin between diseased and healthy tissue. Finally, the system was used in a healthy human subject *in vivo*, demonstrating its ability to acquire stable images with sub-cellular resolution, non-invasively and in real-time. Our results indicate that this type of simple and inexpensive fiber-optic imaging platform can extract qualitative and quantitative information with high-resolution from fluorescently labeled cells and tissues. These capabilities can potentially be used in conjunction with existing and emerging molecular-targeted fluorescent probes, in areas ranging from cell culture studies to clinical imaging in human subjects.

2. Materials and methods

2.1 Fiber-optic microendoscopy system

The primary components of the imaging system are a light source, a fiber-optic bundle, a microscope objective lens, and a CCD camera (Fig. 1(*a*)). The LED light source (Luxeon) produces an optical spectrum centered at 455 nm (20 nm FWHM), and costs less than $5 per unit. A collimator directs light from the LED to the back aperture of a 10x / 0.25 NA infinity-corrected objective lens (Olympus), via a 475 nm cut-off dichroic mirror (Chroma Technology Corp.). Excitation light illuminating the proximal end of a flexible fiber-optic bundle (Sumitomo, IGN-08/30) is transferred coherently to the distal end. The distal tip of the bundle (Fig. 1(*b*)) is placed in direct contact with the sample, delivering 1 mW excitation power. Fluorescence emission from the sample is collected by the bundle, transmitted through the dichroic mirror and imaged onto a CCD camera by a tube lens with magnification factor, *M*. This factor is chosen to balance the conflicting requirements of sampling individual fibers with a sufficient number of pixels at the CCD, whilst confining the magnified image of the bundle to the area of the CCD array. Since the physical size of the bundle determines the field-of-view, the maximum achievable FOV is related to the CCD and bundle properties according to Eq. (1), where w_{CCD} is the CCD size, w_p the pixel size, ϕ_c the fiber core diameter, and n the desired number of samples (pixels) per fiber:

$$FOV_{max} = \frac{w_{CCD}}{w_p}\frac{\phi_c}{n} \tag{1}$$

Two different CCD cameras were evaluated in this work; the results shown in Fig.'s 4 and 5(*a*) were acquired by a scientific-grade color CCD camera (Retiga EXi, QImaging, Inc.), using IEEE 1394 (Firewire) output to directly send continuous image data to a computer. The results shown in Fig's 2, 3, and 5(b) were acquired by a standard analog CCD camera (CV-S3200N, JAI, Inc.), with image acquisition card (National Instruments). Using Eq. (1), the maximum field-of-view at the Nyquist limit (n = 2) is 1416 μm and 539 μm for the Retiga and JAI cameras, respectively. Both cameras use a Bayer mask for color imaging and were digitized at 8-bit resolution. Relevant experimental parameters are summarized in Table 1.

The total cost of the fiber microendoscopy system was $2500 with the standard CCD camera, and $11,000 with the scientific-grade unit.

2.2 3-D cell culture and labeling

Two tyrosine-kinase receptors shown to be overexpressed in epithelial cancers, Her-2 and EGFR, were selected as the antibody targets. Labeling of these extracellular receptors was accomplished using a biotin-antibody conjugate (Neomarkers) and a commercially-available quantum dot-strepatavidin conjugate (Invitrogen). Multiplexed labeling was performed using the two extracellular targets (Her-2 and EGFR) and a green nucleic-acid specific cell dye (SYTO 45, Invitrogen). EGFR was targeted with a red Qdot 655 / streptavidin conjugate, while Her-2 was labeled with a yellow Qdot 585 / streptavidin conjugate. Following labeling, equal numbers of each of these cell types were suspended in collagen. All three fluorophores have spectrally distinct emission spectra but similar absorption spectra, permitting all to be excited with the LED's emission centered at 455 nm. Images of the tri-color fluorescent collagen construct were taking using a 500 nm long-pass filter (Thorlabs) for the green nuclear stain, a 20 nm FWHM bandpass filter centered at 585 nm for the Her-2 fluorophore, and a 20 nm FWHM bandpass filter centered at 655 nm for the EGFR fluorophore (Chroma Technology Corp.). These individual frames were then

uniformly processed by enhancing contrast and applying a false color (ImageJ). Additionally, a fully-multiplexed imaging mode is achieved by using the camera's color imaging capability. A single 500 nm long-pass emission filter was used, with the CCD camera's Bayer mask used to distinguish between each fluorescent cell species.

2.3 Murine tumor model and macroscopic imaging

1483 cells (provided by Dr. P. G. Sacks, New York University College of Dentistry, New York, NY), derived from a human oropharyngeal squamous carcinoma, were injected into the subcutaneous tissue of athymic nude mice. The tumors were grown for approximately 2 to 3 weeks, until they were greater than 5 mm in size, in accordance with a protocol approved by the Institutional Animal Care and Use Committee at Rice University. To visualize the tumor at low resolution within the context of the whole animal, macroscopic imaging was performed using a small animal imaging system (CRI Maestro). To enhance visualization of the tumor in both whole animal imaging and during fiber microendoscopy, the tumor was directly injected with 0.05% acriflavine hydrochloride in PBS. Acriflavine is a non-DNA binding fluorescent molecule that associates with the negatively charged nucleus allowing for optimal visualization of overall tissue architecture. Following a 20 minute incubation period, the skin of the animal was pierced with a 16-gauge needle, and the 1 mm diameter fiber-optic bundle inserted into the tumor. Images and video were acquired while the animal remained under anesthesia. On completion of the microendoscopy imaging, the tumor was removed and subject to routine histologic processing with H&E staining.

2.4 Surgical specimen acquisition and imaging

Through a study protocol approved by both the Rice University and University of Texas M.D. Anderson Institutional Review Boards and following informed consent by the patient, a surgical specimen containing an oral squamous carcinoma located in the buccal mucosa and retromolar trigone was obtained immediately after surgical resection. Acriflavine solution (0.05% in saline) was applied to the mucosa of the specimen, and imaging with the microendoscope followed immediately thereafter. The specimen was subsequently sent for routine histologic processing, which generated H&E stained sections from locations closely corresponding to those imaged with the fiber microendoscope.

3. Results

3.1 System characterization

The spatial resolution of the imaging system is governed by the size and spacing of individual fibers in the coherent bundle. In the system presented here, the fiber core size is 2.2 μm, with a center-to-center spacing of < 4 μm. An image of a standard resolution target demonstrates the system's ability to resolve lines that are 4.4 μm in width (Fig. 2(*a*)). The field-of-view simply corresponds to the active area of the fiber bundle, which is 350 μm in diameter with the fiber bundle used here and 750 μm in the remaining figures in the text.

3.2 Multiplexed imaging

Histopathology typically involves the addition of different chemical stains to individual tissue sections, to generate contrast between tissue components or assess molecular activity under light microscopy. A fundamental goal of *in vivo* molecular imaging is to achieve analogous staining *in situ*, through the use of molecular-targeted fluorophores. The fiber microendoscope can image and distinguish between cells stained with spectrally-distinct fluorescent labels within a single sample. We demonstrated this ability in an *in vitro* system, consisting of three different cancer cell lines, each labeled with a different fluorophore and suspended in a three-dimensional collagen construct. All three fluorophores were excited by

the same LED light source, and individual images were acquired sequentially with three separate emission filters. Following background subtraction, contrast enhancement and false coloring, a composite image was formed, with 1483 cells appearing red, SK-BR-3 cells green, and SiHa cells blue (Fig. 2(*b*)). To distinguish different fluorescent labels simultaneously, the CCD camera's Bayer mask can be used, eliminating the need to exchange separate emission filters and providing real-time multiplexed imaging. This technique is subject to cross-talk due to spectral overlap between the three Bayer mask elements, but the effect can be minimized by use of fluorophores that are as spectrally distinct as possible. The peak wavelengths of the three fluorophores used in this experiment were isolated by at least 50 nm. A single image of the same triple-labeled cell construct was taken with a 500 nm long-pass emission filter (Fig. 2(*c*)). The three cancer cell types can again be differentiated, this time based on correspondence between individual fluorescent emission spectra and the spectral transmission curves for each channel (red, green, and blue) of the Bayer mask.

3.3 *In vivo* tumor imaging

Clinical diagnosis of suspected tumors requires collection of tissue samples for histopathology, an invasive process which must be iteratively repeated when multiple suspicious lesions are present or margin determination is required. Each sample provides information at only one location and at one point in time, leading to sampling error and the need for multiple biopsies at initial and follow-up clinical visits. The flexible, narrow-diameter fiber microendoscope can repeatedly access internal and sub-surface tissue sites in a minimally-invasive fashion. We imaged established subcutaneous tumor xenografts in athymic nude mice after fluorescence labeling, first with a macroscopic imaging system (CRI Maestro), and then with the fiber-optic microendoscope (Fig. 3). Prior to imaging, the tumor was directly injected with acriflavine hydrochloride, a nuclear-associating green fluorescent stain originally used as a topical antiseptic [28], and since as a source of contrast in confocal microscopy [17,18]. The tumor mass was clearly visible with the macroscopic imager (Fig. 3(*b*)). The fiber microendoscope was then introduced into the tumor through the lumen of a 16-gauge needle. As the microendoscope was advanced through the tissue, cellular architecture and morphology could be visualized in real-time (see also Video 1). Nuclei appear as discrete green dots, with continuous green fluorescent regions likely arising from acriflavine uptake in desmoplastic tissue containing fibroblasts within the tumor mass (Fig. 3(*c*)). For direct comparison, an H&E stained histological section (Fig. 3(*d*)) is shown alongside a fiber microendoscope image at the same scale, indicating invasive moderately-differentiated squamous carcinoma cells (dark blue-stained) and reactive desmoplastic (fibrous) tissue from the host response (appearing pink-stained).

3.4 *Ex vivo* human specimen imaging

Histopathologic processing and inspection by an experienced pathologist remains the gold-standard for diagnosis and classification of disease, but there are opportunities for optical imaging to complement established practice in areas such as biopsy guidance and surgical margin detection. In order to demonstrate the ability of the microendoscope system to discriminate and quantify changes associated with cancer, the device was used to image a surgical specimen containing an oral squamous carcinoma located in the buccal mucosa and retromolar trigone. With the fiber microendoscope tip placed in contact with the specimen at a clinically-normal region, bright, sparsely distributed nuclei are visible (Fig. 4(*a*)). In contrast, as the fiber probe was moved to the region clinically-determined to contain the tumor (Fig. 4(*b*)), nuclei qualitatively exhibited the characteristic increase in density and disorganization associated with cancer [29]. Corresponding histopathology sections are also presented and were reviewed by a board-certified pathologist (MDW). The histology in Fig. 4(*a*) demonstrates normal epithelium with some inflammation, while Fig. 4(*b*) indicates the

presence of squamous carcinoma cells extending to the tissue surface. The sub-cellular features which were qualitatively visualized in real-time using the fiber microendoscope were further evaluated by quantitative determination of nuclear-to-cytoplasmic (N/C) ratio, a recognized indicator of cancer and pre-cancer development. The images shown in Fig. 4 were visually inspected, with nuclei outlined manually using image processing software. Pixels in each nuclear region were then assigned a value of 1, with the remainder of the image (corresponding to cytoplasmic area) assigned a value of zero, producing binary images for each sample. Nuclear-to-cytoplasmic ratios were then calculated from the numbers of pixels in each group. Automated image processing techniques may allow for a more rapid and less labor-intensive means of isolating cell nuclei, but for this example, visual identification of nuclei was used to ensure identification of nuclei that were clustered, or in relatively low-contrast regions. The use of the scientific-grade camera, with its improved image contrast, greatly facilitated this process. Images acquired in the tumor region demonstrated a marked increase in N/C ratio compared to the clinically normal region (Fig. 4(c)). The dashed line represents an N/C ratio of 0.08, a threshold value determined by Collier *et al*. for discrimination between normal and cervical intraepithelial neoplasia (CIN) 2/3 in cervical biopsy specimens, through the use of reflectance confocal techniques [29].

3.5 *In vivo* human subject imaging

A growing number of targeted optical contrast agents are gaining approval for human use, raising the prospect of combining molecular-specific fluorescent staining with fiber-optic imaging to perform an optical biopsy in living tissue. We used the fiber microendoscope system to image human tissue *in vivo* in accordance with a protocol approved by the Rice University Institutional Review Board. Following topical application of medical-grade acriflavine (0.05% in saline), the distal tip of the fiber-optic bundle was placed in contact with the normal oral mucosa of a human volunteer. Strong uptake of the fluorescent label is indicated in images by the bright appearance of nuclei and visibility of cell membranes (Fig. 5(*a*)). While this image and those shown in Fig. 4 were acquired with a scientific-grade CCD camera, we also demonstrated the ability of the system to obtain high-resolution images using a low-cost, standard CCD camera. An image of the same *in vivo* tissue is shown in Fig. 5(*b*) (see also Video 2), with cell nuclei still apparent.

4. Discussion

As optical contrast agents capable of indicating the onset of disease at the molecular level transition to pre-clinical and clinical use, techniques for imaging tissue at the sub-cellular level *in vivo* become increasingly relevant. We have developed a fiber-optic microendoscopy system, based around a flexible, 1 mm diameter fiber bundle which can either be placed in direct contact with the site to be imaged, or introduced through a 16-gauge needle for insertion into tissue. The field-of-view and spatial resolution are limited by the physical properties of the fiber bundle; namely the diameter and fiber-to-fiber spacing, which for the system presented here are 750 μm and < 4 μm respectively. For a particular bundle, field-of-view and spatial resolution can be traded-off against each other through the use of additional magnifying lens elements at the distal tip [24,30,31]. This system uses a single LED for fluorescence excitation, and a color CCD camera for image acquisition, enabling multiple fluorescent labels to be visualized in real-time. The utility of imaging with multiple spectral channels was previously demonstrated in fiber bundle confocal imaging of cells labeled with nuclear and cytoplasm-specific fluorophores [24,26]. Here, we used the CCD's built-in Bayer mask to efficiently image three spectral channels simultaneously with a single camera.

Two cameras were evaluated in this study; a scientific-grade cooled CCD (Retiga), and a standard analog CCD (JAI). Both cameras were shown to be capable of sub-cellular resolution imaging, but the direct comparison shown in Fig. 5 reveals differences in image appearance that can be related to camera specifications and the experimental configuration. Sampling at the tissue specimen is determined by the physical spacing of individual fibers in the bundle for direct contact imaging, or the demagnified spacing of these same fibers when an additional objective lens is used at the distal tip. The image appearing at the proximal end of the bundle is then relayed to the CCD camera with magnification factor *M* set by the objective – tube lens combination. For a particular bundle, the number of camera pixels sampling each fiber depends on both the CCD pixel size, and relay magnification, *M*. We summarized these spatial parameters in Table 1. With the JAI camera, the image of each fiber in the bundle spans 1.6 pixels at the CCD sensor, compared to 3.4 pixels per fiber with the Retiga device. So while sampling at the specimen is identical for each camera, the spatial sampling frequency for the intermediate image (at the proximal end of the bundle) is over a factor of two higher with the Retiga CCD and above the Nyquist requirement, resulting in image resolution limited by optical rather than sampling conditions. Intensity resolution is the second factor expected to influence image contrast. While both CCDs were digitized at 8-bit resolution, the higher dynamic range and lower noise figure for the scientific-grade camera results in the least significant bit corresponding to a level times 8.8 times higher than the read noise in the Retiga CCD, compared to only 1.2 times for the JAI camera.

Wide-field fluorescence imaging through a fiber bundle or “image conduit” has been reported previously [22,32,33], with the reduction in optical sectioning strength shown to result in increased collection of background light and reduced image contrast, in comparison with truly confocal techniques [22]. Preliminary tests using a planar fluorescent sample indicated that the fluorescent signal for our system is predominantly collected from a depth of some tens of microns, corresponding to a few cell layers of thickness. However, we have shown here that high-quality images with sub-cellular resolution can nevertheless be obtained with a system that is simple and relatively inexpensive to construct, and robust in operation. Two factors appear to be largely responsible for the high image quality. First, contact imaging inherently eliminates background light that would be generated between the sample surface and the object plane in confocal imaging, and second, use of highly specific, bright fluorophores enables the necessary contrast to be generated between cellular components.

5. Conclusion

We have presented a high-resolution, wide-field fluorescence imaging system based on LED illumination, CCD camera detection, and a 1 mm diameter, flexible fiber-optic bundle. The sub-cellular resolution color imaging capabilities were demonstrated in a series of experiments intended to highlight potential application areas in current clinical practice, and in future applications involving molecular-targeted optical contrast agents. The ability to obtain information from multiple tissue sites over an extended period of time may reduce the inherent uncertainties in point sampling associated with histopathology, and provide additional information on specific molecular expression and activity, biological processes, and an individual’s response to treatment. The instrument retains several of the advantageous features of confocal microscopy, including fiber-optic delivery, real-time image acquisition, and color multiplexing capabilities. In addition, due to its relative simplicity, the instrument is compact, robust, and inexpensive, features which are increasingly valuable in both the research laboratory and clinical setting.

Supplementary Material

Refer to Web version on PubMed Central for supplementary material.

Acknowledgments

We thank Vivian Mack (Rice University) for providing cell samples, cell culture, and small animal handling experience. This work was funded through NIH grants RO1 EB002179 and BRP CA103830.

References and links

1. Weissleder R, Tung CH, Mahmood U, Bogdanov A Jr. In vivo imaging of tumors with protease-activated near-infrared fluorescent probes. Nat Biotechnol. 1999; 17:375–378. [PubMed: 10207887]
2. Ke S, Xiaoxia W, Gurfinkel M, Charnsangavej C, Wallace S, Sevick-Muraca EM, Li C. Near-infrared optical imaging of epidermal growth factor receptor in breast cancer xenografts. Cancer Res. 2003; 63:7870–7875. [PubMed: 14633715]
3. Gao X, Cui Y, Levenson RM, Chung LWK, Nie S. In vivo cancer targeting and imaging with semiconductor quantum dots. Nat Biotechnol. 2004; 22:969–976. [PubMed: 15258594]
4. Becker A, Hessenius C, Licha K, Ebert B, Sukowski U, Semmler W, Wiedenmann B, Grötzinger C. Receptor-targeted optical imaging of tumors with near-infrared fluorescent ligands. Nat Biotechnol. 2001; 19:327–331. [PubMed: 11283589]
5. Jaffer FA, Weissleder R. Molecular imaging in the clinical arena. JAMA. 2005; 293:855–862. [PubMed: 15713776]
6. Massoud TF, Gambhir SS. Integrating noninvasive molecular imaging into molecular medicine: an evolving paradigm. Trends Mol Med. 2007; 13:183–191. [PubMed: 17403616]
7. Flusberg BA, Cocker ED, Piyawattanametha W, Jung JC, Cheung EL, Schnitzer MJ. Fiber-optic fluorescence imaging. Nat Methods. 2005; 2:941–950. [PubMed: 16299479]
8. Kimura S, Wilson T. Confocal scanning optical microscope using single-mode fiber for signal detection. Appl Opt. 1991; 30:2143–2150. [PubMed: 20700189]
9. Giniunas L, Juškaitis R, Shatalin SV. Scanning fiber-optic microscope. Electron Lett. 1991; 27:724–726.
10. Delaney PM, Harris MR, King RG. Fibre-optic laser scanning confocal microscope suitable for fluorescence imaging. Appl Opt. 1994; 33:573–577. [PubMed: 20862051]
11. Dickensheets DL, Kino GS. Micromachined scanning confocal optical microscope. Opt Lett. 1996; 21:764–766. [PubMed: 19876151]
12. Liu JTC, Mandella MJ, Ra H, Wong LK, Solgaard O, Kino GS, Piyawattanametha W, Contag CH, Wang TD. Miniature near-infrared dual-axes confocal microscope utilizing a two-dimensional microelectromechanical systems scanner. Opt Lett. 2007; 32:256–258. [PubMed: 17215937]
13. Shin H-J, Pierce MC, Lee D, Ra H, Solgaard O, Richards-Kortum R. Fiber-optic confocal microscope using a MEMS scanner and miniature objective lens. Opt Express. 2007; 15:9113–9122. [PubMed: 19547251]
14. Seibel EJ, Smithwick QYJ. Unique Features of Optical Scanning, Single Fiber Endoscopy. Lasers Surg Med. 2002; 30:177–183. [PubMed: 11891736]
15. Yelin D, Rizvi I, White WM, Motz JT, Hasan T, Bouma BE, Tearney GJ. Three-dimensional miniature endoscopy. Nature. 2006; 443:765. [PubMed: 17051200]
16. Harris, MR. UK patent. GB 2 340 332 B. 2001.
17. Polglase AL, McLaren WJ, Skinner SA, Kiesslich R, Neurath MF, Delaney PM. Fluorescence confocal endomicroscope for in vivo microscopy of the upper and lower gastrointestinal tract. Gastrointest Endosc. 2005; 62:686–695. [PubMed: 16246680]
18. Kiesslich R, Goetz M, Vieth M, Galle PR, Neurath MF. Technology Insight: confocal laser endoscopy for in vivo diagnosis of colorectal cancer. Nat Clin Pract Oncol. 2007; 4:480–490. [PubMed: 17657253]
19. Gmitro AF, Aziz DJ. Confocal microscopy through a fiber-optic imaging bundle. Opt Lett. 1993; 18:565–567. [PubMed: 19802201]

20. Juškaitis R, Wilson T, Watson TF. Real-time white light reflection confocal microscopy using a fibre-optic bundle. Scanning. 1997; 19:15–19.
21. Liang C, Descour M, Sung K-B, Richards-Kortum R. Fiber confocal reflectance microscope (FCRM) for in-vivo imaging. Opt Express. 2001; 9:821–830. [PubMed: 19424320]
22. Dubaj V, Mazzolini A, Wood A, Harris M. Optic fibre bundle contact imaging probe employing a laser scanning confocal microscope. J Microsc. 2002; 207:108–117. [PubMed: 12180956]
23. Laemmel E, Genet M, Le Goualher G, Perchant A, Le Gargasson J-F, Vicaut E. Fibered confocal fluorescence microscopy (Cell-viZio) facilitates extended imaging in the field of microcirculation. A comparison with intravital microscopy. J Vasc Res. 2004; 41:400–411. [PubMed: 15467299]
24. Jean F, Bourg-Heckly G, Viellerobe B. Fibered confocal spectroscopy and multicolor imaging system for in vivo fluorescence analysis. Opt Express. 2007; 15:4008–4017. [PubMed: 19532645]
25. Sabharwal YS, Rouse AR, Donaldson L, Hopkins MF, Gmitro AF. Slit-Scanning Confocal Microendoscope for High-Resolution In Vivo Imaging. Appl Opt. 1999; 38:7133–7144. [PubMed: 18324260]
26. Rouse AR, Gmitro AF. Multispectral imaging with a confocal microendoscope. Opt Lett. 2000; 25:1708–1710. [PubMed: 18066321]
27. Delaney, P.; Harris, M. Handbook of Biological Confocal Microscopy. 3. Vol. Chap. 26. Springer; New York: 2007.
28. Steinman RR. Pharmacologic Control of Dentinal Fluid Movement and Dental Caries in Rats. J Dent Res. 1968; 47:720–724. [PubMed: 5248911]
29. Collier T, Guillaud M, Follen M, Malpica A, Richards-Kortum R. Real-time reflectance confocal microscopy: comparison of two-dimensional images and three-dimensional image stacks for detection of cervical precancer. J Biomed Opt. 2007; 12:024021. [PubMed: 17477736]
30. Sung K-B, Richards-Kortum R, Follen M, Malpica A, Liang C, Descour M. Fiber optic confocal reflectance microscopy: a new real-time technique to view nuclear morphology in cervical squamous epithelium in vivo. Opt Express. 2003; 11:3171–3181. [PubMed: 19471442]
31. Rouse AR, Kano A, Udovich JA, Kroto SM, Gmitro AF. Design and Demonstration of a Miniature Catheter for a Confocal Microendoscope. Appl Opt. 2004; 43:5763–5771. [PubMed: 15540433]
32. Hirano M, Yamashita Y, Miyakawa A. In vivo visualization of hippocampal cells and dynamics of Ca2+ concentration during anoxia: feasibility of a fiber-optic plate microscope system for in vivo experiments. Brain Res. 1996; 732:61–68. [PubMed: 8891269]
33. Poe GR, Rector DM, Harper RM. Hippocampal Reflected Optical Patterns during Sleep and Waking States in the Freely Behaving Cat. J Neurosci. 1994; 14:2933–2942. [PubMed: 8182449]

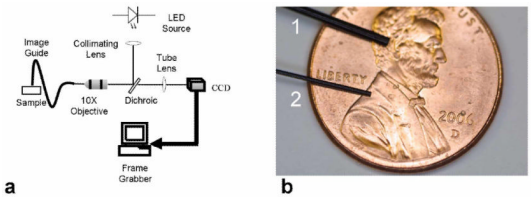

Fig. 1. Fiber-optic microendoscopy system

(a) Schematic diagram. *(b)* Photograph of fiber-optic bundles on a US penny. Bundles 1 and 2 have outer diameters of 1.0 mm and 0.5 mm respectively.

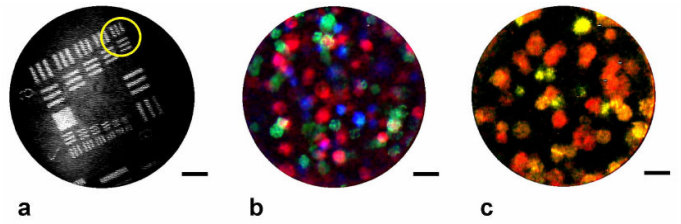

Fig. 2. System resolution and multiplexed cell culture imaging

(a) Image of a standard US Air Force resolution target, demonstrating resolution of the 4.4 μm-wide bars in group 6, element 6 (circled). *(b)* False-color composite image of a 3-D collagen construct containing 1483 oral squamous cell carcinoma cells (red), SK-BR-3 breast cancer cells (green), and SiHa cervical cancer cells (blue), with each cell type stained with a spectrally-distinct fluorophore. *(c)* Single frame image of the same tissue construct acquired in real-time with a single long-pass emission filter. 1483 cells appear red, SK-BR-3 cells yellow, and SiHa cells appear light green. All scale bars represent 50 μm.

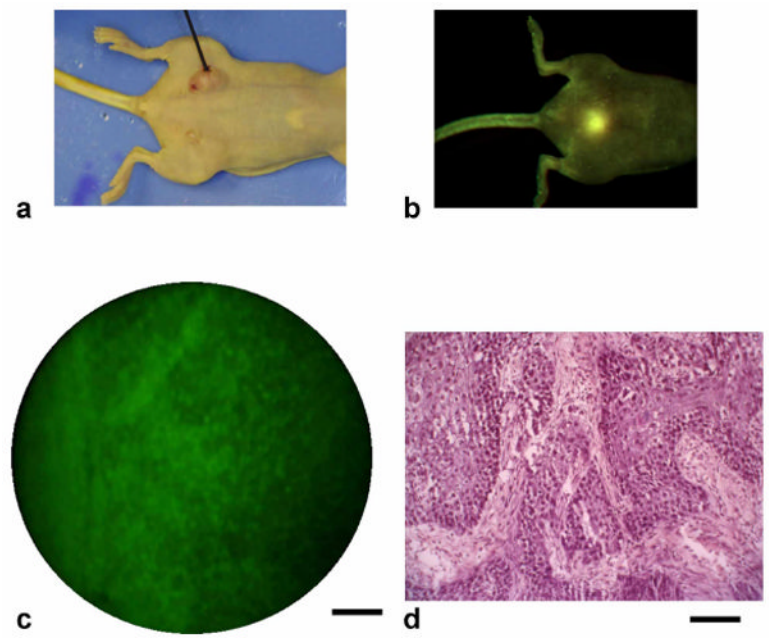

Fig. 3. Murine tumor model imaging

(a) Photograph of an athymic nude mouse showing the fiber microendoscope and subcutaneous tumor. *(b)* Macroscopic fluorescence image (CRI Maestro) acquired following direct injection of fluorescent contrast agent at the tumor site. *(c)* Image acquired by the fiber microendoscope in the living mouse, as the fiber is advanced through the tumor within the lumen of a 16-gauge needle (frame from Video 1, 2.87 MB movie). Tumor cell nuclei appear as bright green dots, with connective tissue within the tumor mass. *(d)* Corresponding histology section following tumor excision. Scale bars represent 100 μm.

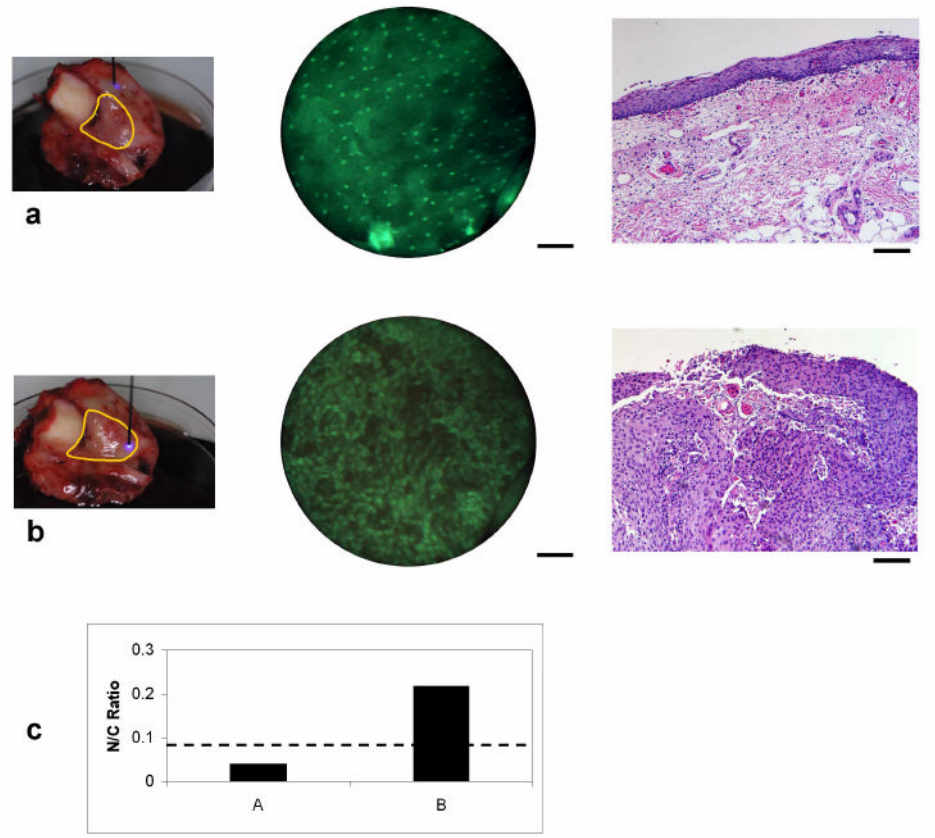

Fig. 4. Surgical specimen imaging

(a) Normal epithelium. Left; photograph of fiber probe in contact with excised tumor tissue. Yellow border represents the clinically-abnormal region identified by the surgeon (AG). Center; microendoscopy image of tissue with probe at location indicated in photograph. Right; corresponding transverse histopathology section from the imaged region. *(b)* Tumor region. Microendoscopy image (center) and histology (right) demonstrate squamous carcinoma throughout the entire epithelium. Scale bars represent 100 μm. *(c)* Graph of calculated nuclear to cytoplasmic ratio for microendoscopy images in *(a, b)*. The dashed line represents an N/C ratio of 0.08.

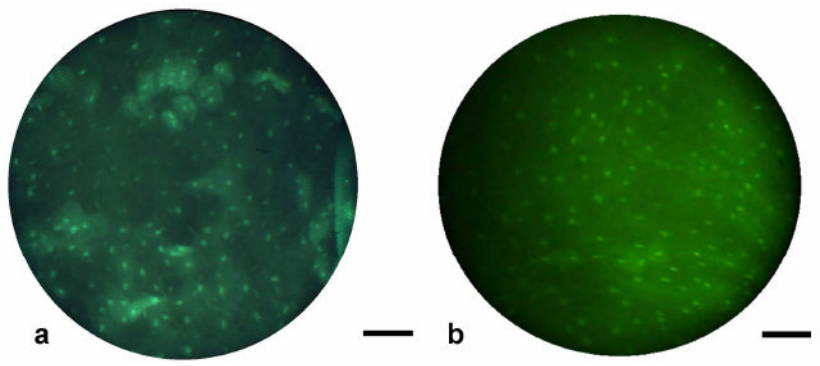

Fig. 5. *In vivo* human tissue imaging

(a) Fiber microendoscopy imaging of normal human oral mucosa *in vivo*, following topical application of fluorescent acriflavine neutral (0.05% in saline). This image was acquired with a scientific-grade CCD camera. *(b)* Image of the same tissue acquired with a standard CCD camera (frame from Video 2, 3.10 MB movie). In both images, cell nuclei appear bright surrounded by dark cytoplasm. Scale bars represent 100 μm.

Table 1

Experimental Parameters For Each CCD Camera

	JAI	Retiga
Array size	6.6 × 4.8 mm	10.2 × 8.3 mm
Pixel size	8.4 × 9.8 μm	6.45 × 6.45 μm
Number of pixels	768 × 494	1392 × 1040
Relay magnification, *M*	7x	10x
Pixels per fiber at CCD	1.6	3.4
Dynamic range	50 dB	67 dB
Least significant bit at 8-bit A/D*	$1.2\sigma_{read}$	$8.8\sigma_{read}$

*Read noise, σ_{read}